J Mater Sci (2007) 42:5256–5263
DOI 10.1007/s10853-006-0369-0

# Deformation and fracture behavior of electrocodeposited alumina nanoparticle/copper composite films

**Yong X. Gan · Chih-Shing Wei · Marca Lam · Xiaoding Wei · Dongyun Lee · Jeffrey W. Kysar · Xi Chen**

Received: 20 September 2005 / Accepted: 24 April 2006 / Published online: 31 January 2007


**Abstract** Electrocodeposition of alumina nanoparticles and copper thin film on silicon wafers was performed. The volume fraction of the nanoparticle is about 5% and the size is about 50 nm. Comparison between the static tensile behaviors of specimens with and without nanoparticles reveals that the Young's modulus is significantly increased by incorporating nanoparticles into the copper film. However, the ultimate tensile strength of the nanocomposite (235 MPa) is slightly lower than that of the pure copper reference specimen (250 MPa). For the nanocomposite, the strain at failure is 7.8%, which is lower than that of the pure copper film (10.5%). Distinct microscale deformation mechanisms are observed: the main deformation mechanism of the pure copper film is slip followed by strain hardening, whereas for the nanocomposite, multistage failure behaviors are found due to the debonding at the nanoparticle/copper interface. Notched specimens were also tested and compared with the unnotched specimens. In addition, cyclic loading tests on the nanocomposite were conducted to show its hardening behavior.

Y. X. Gan (✉) · C.-S. Wei
Department of Mechanical Engineering, Albert Nerken School of Engineering, The Cooper Union for the Advancement of Science and Art, 51 Astor Place, New York, NY 10003, USA
e-mail: gan@cooper.edu

M. Lam
Department of Chemical Engineering, Albert Nerken School of Engineering, The Cooper Union for the Advancement of Science and Art, 51 Astor Place, New York, NY 10003, USA

X. Wei · D. Lee · J. W. Kysar
Department of Mechanical Engineering, Fu Foundation School of Engineering and Applied Science, Columbia University, 500 West 120th Street, New York, NY 10027, USA

X. Chen
Department of Civil Engineering and Engineering Mechanics, Fu Foundation School of Engineering and Applied Science, Columbia University, 500 West 120th Street, New York, NY 10027, USA

## Introduction

Electrocodeposition is an efficient method to incorporate particles into metallic coatings. Many researchers have demonstrated that nanoparticles/copper or copper alloy composite materials could be prepared with the electrocodeposition technique [1–5]. For example, electrocodeposition of nanometer-sized alumina particles in a copper matrix was studied using a concentric cylindrical electrode configuration [6]. The electrode was set up in a manner such that the particle incorporation into films occurred on either the interior rotating or outer stationary cylinder [7, 8]. Afshar et al. [9] obtained composite coatings of bronze (90% Cu–10% Sn) with 8.5% (vol) graphite particles from an alkaline bath containing cyanide. Composite copper coatings encompassing lubricating oil microcapsules were prepared by Zhu and Zhang [10], in which the codeposition mechanisms and functions of the composite coating were emphasized. Recently, we have demonstrated the feasibility of the electrocodeposition of nanosized alumina particles and copper thin films on silicon wafers with pre-coated conductive surface

layers [11]. The electrochemical reaction behavior of the codeposition of copper and particles was also studied [12].

Different types of electrolyte were developed as replacements of sulfate to facilitate the deposition of alloy elements into the copper matrix. For example, a pyrophosphate bath was proposed using chloroplatinic acid as a source of platinum so that platinum can be introduced into the copper coating [13]. The electrocodeposited composites have found many potential applications owing to their cost-effectiveness and good physical properties [14]. For example, the electrocodeposited composites exhibit shape-complexity with controlled tolerances, which may be employed in tooling, mould making [15], micro- or nanoscaled fabrication [16], and microelectromechanical systems (MEMS) [17]. In addition, when combined with lithography, electrocodeposition and plastic moulding became very useful in MEMS fabrication [18, 19]. Applications in microoptics and medicine were also performed as reported by MacGeough et al. [20].

The physical and mechanical properties of electrodeposited copper can be significantly changed by incorporating different types of particle and varying the volume fraction of the particles. In the work performed by Zhu et al. [21], silicon carbide particle (SiCp) reinforced copper-based composites were prepared by electroforming to study the mechanical properties of the composites. The effects of the concentration of SiCp in the plating solution, temperature, and current density were also examined. Through the optimization of the processing parameters, the increase of SiCp content in the composite was effectively controlled during the codeposition process. The mechanical properties of Cu/SiCp composites were improved with the addition of SiCp, where higher Vickers hardness (HV) and bending strength were observed with the increase of the particle volume fraction. Residual stresses were also reported in the electrocodeposited Cu/SiCp composites.

The mechanical properties of the nanocomposites, such as the Young's modulus, may be determined in various ways. Indirect measurements, such as the micro- and nanoindentation tests, are commonly used to obtain the elastic stiffness of bulk materials and thin films. At present, direct experiment on the nanoparticle reinforced copper composites, such as the microtensile test, is still lacking. In this paper, we report the mechanical properties of electrocodeposited nanoparticle-copper thin composite films by using the microtensile test. Both static and cyclic tensile tests on the nanocomposite thin film specimens are carried out where the specimens are fabricated through the microfabrication technology. The effects of adding nanoparticles into the copper thin films are studied by comparing the mechanical properties of the materials with and without nanoparticles via the static microtensile test.

The content of this paper is divided into three sections. In the first section, we describe the electrocodeposition of nanometer-sized alumina particles with copper coatings on silicon wafers, where a surface conductive gold layer is deposited by thermal evaporation. In the second section, static microtensile tests of the nanocomposite and pure copper films are presented, and the comparison between these specimens reveals the improvement of the mechanical properties by incorporating nanoparticles. In the last section, concluding remarks are elaborated.

## Materials and experimental methods

### Materials

Silicon wafers with the dimensions of 75 mm in diameter and 0.3 mm in thickness were acquired from Nova Electronic Materials, Ltd., Carrollton, Texas, USA. The wafers are in test grade with one side being mechanically and chemically polished. The polished side is used for thin film deposition in the subsequent experiments. Copper (II) sulfate ($CuSO_4 \cdot 5H_2O$) with purity of A.C.S. standard is obtained from Alfa Aesar, Ward Hill, Maryland, USA. The sulfuric acid was acquired from Fisher Scientific with the grade of Certified A.C.S. plus. The anode used for electrocodeposition is a high purity copper plate. The nanoparticles are gamma typed alumina made by Buehler, Lake Bluff, Illinois, USA. A gold wire with a diameter of 0.8 mm was used as the target material for thermal evaporation deposition, which is obtained from Alfa Aesar, a Johnson Matthey Company, Ward Hill, MD, USA.

### Preparation of conductive thin films

The silicon wafers were cleaved into long strips. Thermal evaporation deposition of gold films onto the polished side of the wafer strips was conducted first to provide an electrically conductive surface on which the nanocomposite thin film can be subsequently electrocodeposited. In order to prepare the dog-bone-shaped tensile specimens, microfabrication technologies were used to pattern the conductive gold thin film. First, a stainless steel sheet was cut into a shadow mask using an RA90 electrical discharge machine (EDM), manufactured by

Mitsubishi Corporation. The shadow mask with an opening window of a dog-bone shape was clamped together with a silicon wafer as shown in Fig. 1. Gold thin film with thickness of about 20–25 nm was deposited onto the polished side of the silicon wafer via the opening window of the mask. During this process, the vacuum level is maintained at $2.4 \times 10^{-6}$ Torr, and the thickness of the conductive layer was measured using a Dektak Profilometer. The electrical conductivity across the Au films is about $5.5 \times 10^{-8}$ Ωm, which meets the conductive requirements as the cathode for the subsequent electrocodeposition.

## Electrocodeposition

Figure 2 sketches the experimental set-up for electrocodeposition. The electrolyte contains a mixture of copper (II) sulfate ($CuSO_4 \cdot 5H_2O$) and sulfuric acid. The $Al_2O_3$ nanoparticles used in this study have an average diameter of approximately 50 nm. The electrochemical cell used for electrocodeposition is a 500 ml cylindrical glass beaker. The anode is a pure copper plate and the cathode is the aforementioned silicon wafer with gold coating, and they face each other in parallel at a distance of about 50 mm. On the bottom of the cylindrical beaker, an electromagnetic stirring bar encapsulated in Teflon coating rotates at 300 rpm, such that the agitation of the solution helps to keep the $Al_2O_3$ nanoparticles suspended in the solution during the electrocodeposition process. The deposition parameters such as temperature, voltage and current density were optimized, which are deduced as: plating temperature of 50 °C; voltage of 2.5 V; and the current density of 150 A/m$^2$. The deposition rate is estimated to be about $4.5 \times 10^{-3}$ μm/s using the Faraday's law.

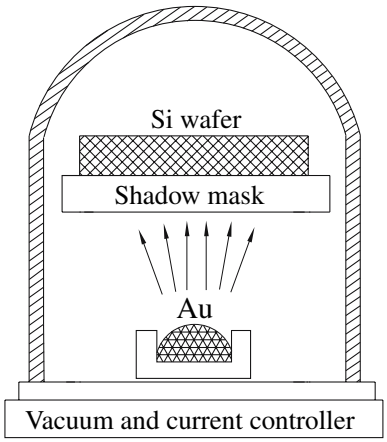


**Fig. 1** Schematic of coating the gold thin film by thermal evaporation

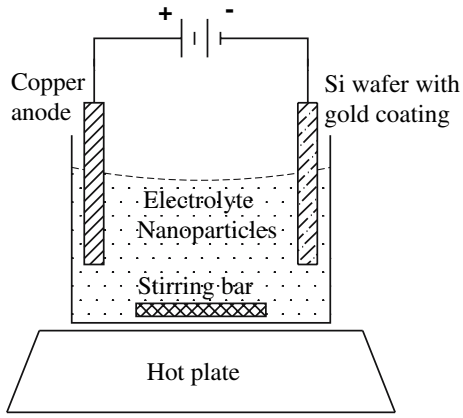


**Fig. 2** The set-up of electrocodeposition experiment

The thickness of the Cu–$Al_2O_3$ nanocomposite on the silicon substrates was kept to be about 220 ± 5 μm. As a control reference specimen, pure copper was electrodeposited onto silicon substrates under the same conditions. Following the deposition procedures, removing of the silicon wafer substrate through wet etching was performed in a 20 wt% NaOH solution at 90 °C for 2 h. After being cleaned in deionized water, the specimens to be used in the microtensile tests were obtained.

## Mechanical property testing

Mechanical property tests were performed under load-controlled conditions using a materials testing system (MTS 810) with a 548 controller. The dimensions of the dog-bone shaped specimens are specified in Fig. 3, which have a gauge length of 20 mm, a width of 5 mm, and a thickness of 0.22 mm. During the testing, the load and displacement data were recorded in situ by a LabView program and subsequently processed using MATLAB programs, which converts the load–displacement curves into stress–strain plots. Tensile tests on notched specimens were also performed to examine the toughness of the nanocomposite and control specimens. Cyclic loading–unloading tests were

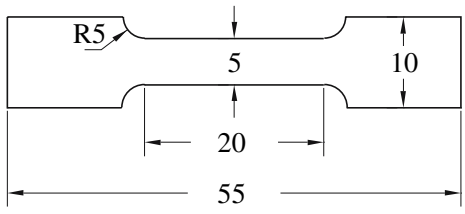


**Fig. 3** The geometry of the microtensile test specimens (the unit is mm)

conducted to obtain the hysteresis loops related to the plastic deformation of the nanocomposite thin film material.

### Microscopic examination

The electrocodeposited nanocomposite and pure copper thin film specimens were examined using the scanning electron microscopy (SEM). Two types of images were taken: the secondary electron (SE) images and backscattering electron (BE) images. The low magnification SE images were taken using the JEOL 5600 electron microscope in the Materials Research Science and Engineering Center (MRSEC) at Columbia University. High resolution BE images were taken with a Hitachi S4700 SEM in the Nanoscience and Engineering Research Center at Columbia University. Before the microscopic examination, the surface of the nanocomposites was electropolished in an 85% orthophosphate solution and dipped shortly in a 33% nitric acid methyl alcohol solution for 2–3 s to expose the particles, such that they can be easily observed under the SEM.

## Results and discussions

### Static tensile properties

#### *Unnotched specimens*

Figure 4(a) shows the stress–strain relationship of the alumina particle/copper composite material. It is noted that the ultimate tensile strength of the nanocomposite is about 235 MPa, and the strain at failure is about 7.8%. By contrast, Fig. 4(b) shows the tensile characteristic of the control copper thin film, which is obtained by electrodeposition under the same conditions as the nanocomposites; its ultimate tensile strength is 250 MPa and the strain at failure is about 10.5%. The data indicate that with the addition of nanoparticles, the copper becomes less ductile.

In order to reveal the increase of stiffness due to the addition of the nanoscale particles, statistics analysis is performed based on the data from multiple tests. The yield stress is defined at the 0.2% offset in the stress–strain relationship (c.f. Fig. 4), and the deformation prior to yield is assumed to be elastic, where the Young's modulus can be derived as the averaged slope of the elastic portion of the stress–strain curve. We measured ten pure copper thin film specimens and their Young's moduli were calculated with a mean value of 120 GPa, and a standard derivation of 6 GPa. By contrast, ten nanocomposite thin film specimens were tested. The mean Young's modulus of the nanoparticle reinforced copper thin film is 139 GPa, with a standard deviation of 9 GPa. Comparison of such results reveals the significant increase of the Young's modulus after the addition of the nanoparticles in copper matrix, which is caused in part by the rule of mixture of the composite, and in part by the resistance of copper dislocation movement exerted from the pinned nanoparticles. The increment of the Young's modulus due to the rule of mixture can be estimated to be about 4 GPa (by taking the modulus of $Al_2O_3$ to be 390 GPa and the 5% volume fraction). The remaining stiffening effect is possibly related with the early stage of dislocation movement. In copper, the 12 possible slip systems, $\langle 110\rangle/\{111\}$, can be activated once the local shear stress reaches a critical value, which may occur at a very low stress level in the nanocomposite due to the stress concentration in the vicinity of the nanoparticle. Therefore, even during the initial elastic deformation (when the plastic strain is less than 0.2%), the stress–strain behavior is not strictly linear and dislocation slip is likely activated. Some of the nanoparticles located within the copper grains are obstacles which impede the slip, while other particles on the grain boundaries can further prevent the dislocation sliding along the grain boundaries; both

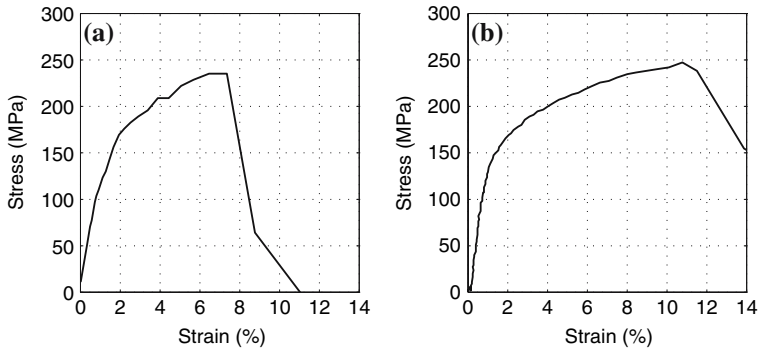


**Fig. 4** The stress–strain relationship measured from unnotched specimens (**a**) $Al_2O_3$/Cu nanocomposites, (**b**) pure copper thin films

mechanisms not only increase the yield stress and ultimate tensile strength, but also increase the stress during elastic deformation and raise the Young's modulus of the nanoparticle reinforced metal. Thus, the calculated Young's modulus for the composite materials is higher than that for the pure copper matrix material.

The standard derivation of the Young's modulus measured for the nanocomposites is about one and half times higher than that for the pure copper specimens, which is possibly due to the localized plastic deformation around the nanosized particles. In the composite material, dislocation movements are activated preferentially around the particles due to stress concentration. Since the nanoparticle distribute in the materials randomly and the volume fraction of nanoparticles is relatively low (5%), each individual specimen may exhibit different stress values at the strain level corresponding to the initiation of the plastic flow. Thus, the calculated values of the Young's moduli of the nanocomposites show higher standard derivation than that of the control specimens. The results also indicate that the scatter of the mechanical property of the composite is higher than that of the pure copper.

The ultimate tensile strength of the composite material is slightly lower than that of the control pure copper thin films, which may be related to the debonding at the nanoparticle–matrix interface at high strain levels. Once the interfacial debonding occurs, nanoparticles cannot take the role of reinforcement; instead, they become defects in the matrix, which reduce the load carrying capability of the material. This is confirmed by the shape of the stress–strain curve shown in Fig. 4(a), which exhibits multistage failure behaviors, as revealed by the small plateaus following yielding that are typical characteristics of particle/matrix interface debonding. Nevertheless, only the easy gliding feature followed by uniform hardening is found in Fig. 4(b), which is typical in the deformation of face-centered cubic (FCC) copper and copper alloys.

*Notched specimens*

Tensile test is performed on the single-edge notched specimens made by the nanocomposite and pure copper. The notch is introduced by EDM cutting with brass wire which has a diameter of 0.015 mm. Figure 5(a) shows the average result from three nanocomposite thin film specimens with a notch depth to specimen width ratio ($a/w$) of 0.165. The major information that can be obtained from the tensile test is the toughness of the materials. Following the equation given by fracture mechanics, we have:

$$J_{\mathrm{Ic}} = C\sigma\sqrt{\pi a} \tag{1}$$

where $a$ is the crack length, $J_{\mathrm{Ic}}$ is the fracture toughness, $\sigma$ is the stress at failure, and $C$ is a constant related with the notch configuration.

If the specimen has a single-edged through-thickness notch, the value of $C$ may be calculated using the relationship derived in [22] as

$$C = f\left(\frac{a}{W}\right)\sqrt{\frac{W}{\pi a}} \tag{2}$$

The geometrically determined term, $f(a/w)$, is given by [22]:

$$f\left(\frac{a}{W}\right) = \frac{\sqrt{2\tan\left(\frac{W}{\pi a}\right)}}{\cos\left(\frac{W}{\pi a}\right)} \left\{0.752 + 2.02\left(\frac{a}{W}\right) + 0.37\left[1 - \sin\left(\frac{W}{\pi a}\right)\right]^3\right\} \tag{3}$$

From the result shown in Fig. 5(a), the maximum stress value of 160 MPa can be obtained, from which

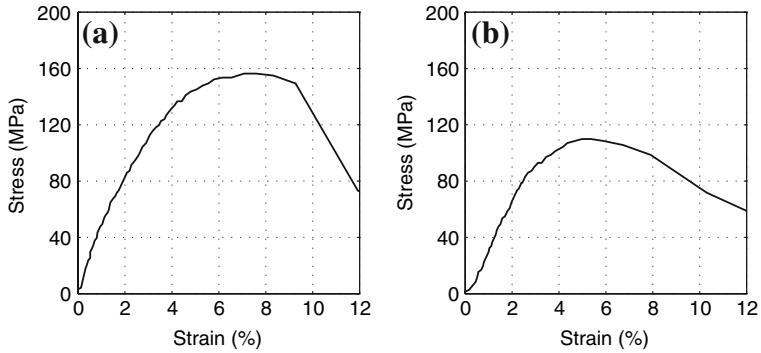


**Fig. 5** The stress–strain relationship measured from notched specimens (**a**) $Al_2O_3$/Cu nanocomposite ($a/w$ = 0.163), (**b**) pure Cu thin film ($a/w$ = 0.263)

the fracture toughness of the nanocomposite can be estimated as 15.26 MPa√m. Another batch of notched nanocomposite specimens with $a/w = 0.263$ were also tested, where the average fracture toughness is derived to be about 11.59 MPa√m.

As a comparison, the averaged tensile behavior of the notched pure copper thin film specimen with $a/w = 0.263$ is also shown in Fig. 5(b). From the highest point on the curve, we can determine the stress at failure to be about 110 MPa, which leads to the critical stress intensity factor of 12.89 MPa√m. Comparison of the calculated $J_{Ic}$ of the nanocomposite and the pure copper specimens (with the same dimension and notch) reveal that the nanocomposite is slightly more brittle, which is consistent with the measurement of ultimate tensile strength and strain at failure as discussed in section ''Static tensile properties''.

## Microstructure

Figure 6 shows the typical morphology of the nanoparticles reinforced copper thin film composite. This image is taken using a backscatter detector in the Hitachi S4700 field emission SEM, where the small black dots represent nanoparticles and dark lines are the grain boundaries (location ''A'' in the backscattering SEM micrograph of Fig. 6). The contrast of the micrograph is determined by the composition of the specimen under examination. Although the surface of the specimen is fairly smooth, the grain boundaries are shown owing to the composition difference between the materials in the grains and the materials along the grain boundaries. From the image contrast analysis, the volume content of the alumina particles in the copper matrix is confirmed to be approximately 5%. It can be readily seen from Fig. 6 that some of the nanoparticles are distributed along grain boundaries while others locate inside the grains. The particles within the grains are expected to be very effective in resisting the movement of dislocations. The particles dispersed along the grain boundaries have two functions. One of such functions is to impede the grain boundary sliding due to the higher specific modulus of the nanoparticle than that of the copper matrix, which is expected to be beneficial to increase the creep resistance of the materials. Another function is that these particles can suppress the growth of the copper grains during the electrocodeposition process. Thus, the existence of the inter-granular particles can refine the grains of the matrix, which has been shown in our earlier work [11]. According to the Hall–Petch relationship, the yield stress is expected to be higher for the nanocomposite whose grains are finer than the control pure copper. The results from morphological analysis are in agreement with the mechanical testing data as shown in Fig. 4.

Secondary electron microscopic image of the same specimen was taken and shown in Fig. 7, where the alumina particles are revealed as white spots, and the copper matrix is shown as the dark-shaded background. The nanocomposite specimen was electropolished in an 85% orthophosphate solution and etched shortly in a 33% nitric acid methyl alcohol solution. Since there is no chemical composition information carried by a secondary electron microscopic image, the grain boundaries cannot be seen as clearly as that in the backscattering SEM image of Fig. 6. From the morphology shown in Fig. 7, it is found that

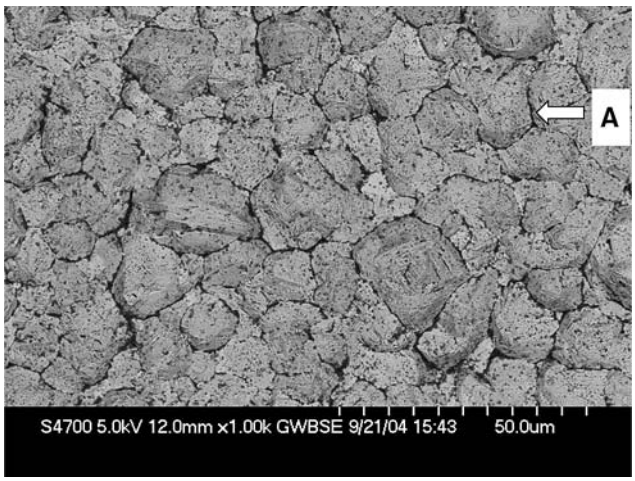


**Fig. 6** Backscatter electron microscopic image of the $Cu/Al_2O_3$ nanocomposite

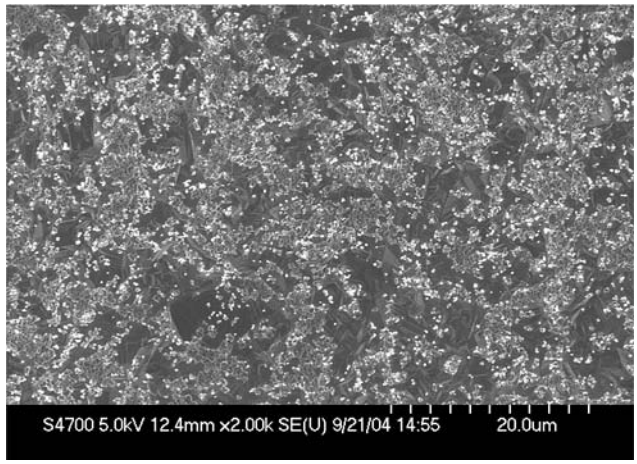


**Fig. 7** Secondary electron microscopic image of the $Cu/Al_2O_3$ nanocomposite

the nanoparticles disperse into the matrix randomly, and the particle aggregation is not severe. Such a morphological feature is very important for the improvement of the mechanical properties of the composite material.

## Fracture surface morphology and failure mechanisms

The fracture surface morphology of the nanocomposite is shown in Fig. 8, which exhibits a hybrid ductile/brittle fracture mechanism. It is noticed that the alumina nanoparticles in the copper matrix have changed the microscaled deformation mechanism of the material. In a pure copper specimen, the fracture surface morphology is typically characterized by numerous dimples and void coalescence zones due to the good ductility of the FCC crystalline structure of copper. However, in Fig. 8, some cleavage features such as the laminar separation (location "A" in the secondary electron micrograph) and the cleavage facets (location "B" in the micrograph), are shown along with the ductile mechanisms including the elongated grains (location "C" in the micrograph) and the tearing ridges (location "D" in the micrograph). From the tensile test data for pure copper thin film (Fig. 4(b)), easy gliding with limited hardening can be identified from the stress–strain relationship, whereas the nanocomposite demonstrates a multistage failure characteristic which may be caused by the debonding of the nanoparticle/copper interface (shown in Fig. 4(a)). Thus, the features on fracture surface morphology are in agreement with the results shown by the tensile test data in Fig. 4.

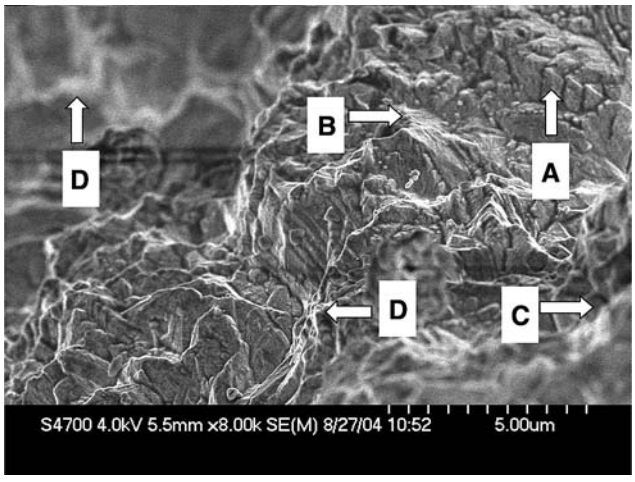


**Fig. 8** Fracture surface morphology of the nanocomposite

## Deformation behavior under cyclic loading

Cyclic loading test on a notched nanocomposite thin film ($a/w = 0.246$) was performed under load controlled conditions, where the average stress level is $\sigma_a = 40$ MPa, and the minimum-to-maximum stress ratio $R = \sigma_{min}/\sigma_{max} = 0.075$. During the first cycle, the nanocomposite shows a notch-opening feature, as well as a typical stress–strain behavior for ductile FCC metals. Figure 9(a) shows the stress–strain relationship based on the calculation, by using the specimen area before the notch is cut.

Figure 9(b) describes the stress–strain curve of the nanocomposite material during the second stage of fatigue loading. The Young's modulus calculated from this cycle is higher than 300 GPa, which is surprisingly high for copper-based materials. Since the Young's modulus of the nanocomposite is around 145 MPa during the initial loading cycle, the significant increase of the elastic modulus is caused by the work hardening of the material under plastic deformation.

In the third cycle of loading, the material demonstrated no appreciable hardening compared with the second cycle. Thus, it is postulated that the fatigue damage of the material is stabilized since the third cycle, with a typical hysteresis similar to that shown in Fig. 9(b). In this stage, since the variation of the stiffness of the nanocomposite is not significant, the amount of plastic deformation energy absorbed by the material remains essentially constant.

The nanocomposite material shows the ductile tearing behavior during the fourth stage of cyclic loading. We capture the unstable ductile tearing of the composite material until failure, when the separation of the two parts of the nanocomposite specimen has just occurred. As shown in Fig. 9(c), the last cycle of the loading behavior is similar to the failure behavior of the composite material under static loading test as shown in Fig. 4(a).

## Conclusion

1. Nanometer-sized alumina particles with copper coatings are electrocodeposited on silicon wafers. The nanocomposite thin film is produced using a sulfuric copper solution with a volume content of the alumina particles of about 5%.
2. Mechanical property characterization of the nanocomposite shows that there is about 10–15% increase of the Young's modulus due to the existence of nanoparticles in the copper matrix. However, the ultimate tensile strength of the composite, 235 MPa,

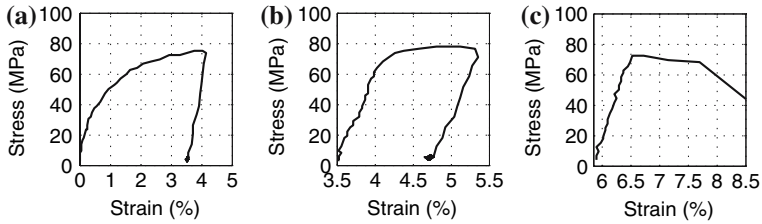


**Fig. 9** The stress–strain relationship of notched $Al_2O_3$/Cu nanocomposite specimens under cyclic loading (**a**) during the first cycle, (**b**) during a cycle in the stable fatigue damage stage (**c**) at fatigue failure (the last cycle)

is slightly lower than that of the pure copper thin film obtained by electrodeposition under the same conditions, which is about 250 MPa. The strain at failure for the nanocomposite is 7.8%, which is smaller than that of pure copper 10.5%, indicating that the nanocomposite is less ductile.

3. The incorporation of alumina nanoparticles in the copper matrix changes the microscale deformation mechanism of the material. For pure copper thin film, easy gliding with limited hardening is revealed by the stress–strain relationship, whereas the nanocomposite demonstrates a multistage failure feature, which may be caused by the debonding of the nanoparticle/copper interface.
4. Preliminary testing results of the notched specimens indicate that the fracture toughness of the nanocomposite is slightly smaller than that of pure copper thin films, thus confirming it is slightly more brittle. The results of cyclic tensile loading tests on the nanocomposite show the hardening behavior of the material under the reversed plastic deformation. In the last stage of the cyclic loading, the ductile tearing behavior is observed.

**Acknowledgments** This work was supported in part by MRSEC Program of the National Science Foundation under Award Number DMR-0213574 and by the New York State Office of Science, Technology and Academic Research (NYSTAR). YXG appreciates Mr. Richard J. Harniman in the Nanoscience and Engineering Center, Columbia University for his valuable assistance in using the Hitachi S4700 scanning electron microscope. We also appreciate both the editor and the reviewers for providing valuable comments for modification on the paper.

## References

1. Buelens C, Celis JP, Roos JR (1983) J Appl Electrochem 13:541
2. Greco VP (1989) Plat Surf Finish 76:68
3. Lee CC, Wan CC (1988) J Electrochem Soc 135:1930
4. Chen ES, Lakshmin GR, Sautter FK (1971) Metall Trans 2:937
5. Groza JR, Gibeling JC (1993) Mater Sci Eng A 171:115
6. Stojak JL, Talbot JB (2001) J Appl Electrochem 31:559
7. Talbot JB (2004) Plat Surf Finish 91:60
8. Stojak JL, Talbot JB (1999) J Electrochem Soc 146:4504
9. Afshar A, Ghorbani M, Mazaheri M (2004) Surf Coat Technol 187:293
10. Zhu LQ, Zhang W (2004) Acta Physico-Chim Sin 20:795
11. Gan Y, Lee D, Chen X, Kysar JW (2005) J Eng Mater Technol 127:451
12. Celis JP, Roos JR (1977) J Electrochem Soc 124:1508
13. Obert J, Lalvani SB (2004) J Appl Electrochem 34:397
14. Greco VP (1989) Plat Surf Finish 76:62
15. Watson S (1989) Trans Inst Metal Finish 67:89
16. Lyshevski SD (2002) MEMS and NEMS. CRC Press, Boca Raton, p 411
17. Beeby S, Ensell G, Kraft M, White N (2004) MEMS mechanical sensors. Artech House, Inc., Boston, p 33
18. Franssila S (2004) Introduction to microfabrication. John Wiley and Sons, Ltd., Chichester, p 218
19. Lyshevski SD (2005) Nano- and micro-electromechanical systems, fundamentals of nano- and microengineering. CRC Press, Boca Raton, p 657
20. MacGeough JA, Leu MC, Rajurkar KP, De Silva AKM, Liu Q, (2001) CIRP Ann Manuf Technol 50:499
21. Zhu JH, Liu L, Hu GH, Shen B, Hu WB, Ding WJ (2004) Mater Lett 58:1634
22. Anderson TL (1991) Fracture mechanics fundamentals and applications. CRC Press, Boca Raton, p 714